MOLECULAR AND CELLULAR BIOLOGY, July 2011, p. 3019–3028 Vol. 31, No. 14
0270-7306/11/$12.00 doi:10.1128/MCB.05178-11

Chondrocyte-Specific MicroRNA-140 Regulates Endochondral Bone Development and Targets *Dnpep* To Modulate Bone Morphogenetic Protein Signaling[▽]

Yukio Nakamura,[1] Jennifer B. Inloes,[2] Takenobu Katagiri,[3] and Tatsuya Kobayashi[2]*

Clinical Research Center, Murayama Medical Center, Tokyo 208-0011, Japan[1]; Endocrine Unit, Massachusetts General Hospital, and Harvard Medical School, Boston, Massachusetts 02114[2]; and Division of Pathophysiology, Research Center for Genomic Medicine, Saitama Medical University, Hidaka, Saitama 350-1241, Japan[3]

Received 8 February 2011/Returned for modification 6 March 2011/Accepted 8 May 2011

MicroRNAs (miRNAs) play critical roles in a variety of biological processes in diverse organisms, including mammals. In the mouse skeletal system, a global reduction of miRNAs in chondrocytes causes a lethal skeletal dysplasia. However, little is known about the physiological roles of individual miRNAs in chondrocytes. The miRNA-encoding gene, *Mir140*, is evolutionarily conserved among vertebrates and is abundantly and almost exclusively expressed in chondrocytes. In this paper, we show that loss of *Mir140* in mice causes growth defects of endochondral bones, resulting in dwarfism and craniofacial deformities. Endochondral bone development is mildly advanced due to accelerated hypertrophic differentiation of chondrocytes in *Mir140*-null mice. Comparison of profiles of RNA associated with Argonaute 2 (Ago2) between wild-type and *Mir140*-null chondrocytes identified *Dnpep* as a *Mir140* target. As expected, *Dnpep* expression was increased in *Mir140*-null chondrocytes. *Dnpep* overexpression showed a mild antagonistic effect on bone morphogenetic protein (BMP) signaling at a position downstream of Smad activation. *Mir140*-null chondrocytes showed lower-than-normal basal BMP signaling, which was reversed by *Dnpep* knockdown. These results demonstrate that *Mir140* is essential for normal endochondral bone development and suggest that the reduced BMP signaling caused by *Dnpep* upregulation plays a causal role in the skeletal defects of *Mir140*-null mice.

MicroRNAs (miRNAs) are endogenously produced, small RNAs that regulate gene expression mainly at the posttranscriptional level. Direct binding of miRNAs to their target RNAs usually suppresses gene expression and facilitates RNA degradation (1, 3, 39). It is suggested that miRNAs act not only as genetic buffers to suppress harmful leaky gene expression that may compromise the robustness of cellular phenotypes but also as drivers of phenotypical diversity (14). miRNAs have been shown to regulate important biological functions in diverse organisms, including mice (33). In mouse chondrocytes, global miRNA deficiency caused by conditional ablation of *Dicer*, a gene encoding an RNase III that catalyzes miRNA maturation, results in reduced proliferation and accelerated hypertrophic differentiation downstream of the parathyroid hormone-related peptide (PTHrP) signaling pathway, presumably at a level that inhibits premature hypertrophic differentiation (20). Because chondrocytes express several hundred detectable miRNAs, it is unclear which particular miRNAs are responsible for the skeletal defects of *Dicer*-deficient chondrocytes. Clarifying the physiological roles of individual miRNAs in chondrocytes is critical for us to further understand the miRNA-mediated gene regulatory system in the skeletal system and to ultimately harness this system for treatment of skeletal diseases.

MicroRNA-140 (miR-140) and -140*, encoded by the *Mir140* gene, are expressed almost exclusively in chondrocytes (38, 40). *Mir140* is evolutionarily conserved among vertebrates, but this gene is not present in invertebrates. These findings suggest that *Mir140* confers certain advantages to vertebrate skeletal systems.

A previous study using zebrafish embryos demonstrated that miR-140 regulates palate chondrogenesis by inhibiting the expression of platelet-derived growth factor receptor, alpha polypeptide (PDGFRA) (9). Deregulation of PDGFRA signaling appears to influence the migration of neural crest-derived mesenchymal cells to the rostral region, which subsequently affects the formation of cartilaginous elements of the head. However, this study provides little insight into the role of *Mir140* in chondrocytes, the major cell type expressing this miRNA gene.

In order to understand the physiological role of *Mir140*, we generated *Mir140*-null mice. Mice lacking *Mir140* showed a shortening of endochondral bones, likely due to mildly accelerated chondrocyte differentiation into postmitotic hypertrophic chondrocytes. Furthermore, we have experimentally identified *Dnpep* as a *Mir140* target whose upregulation may play a causal role in the skeletal defect of *Mir140*-null mice by dampening bone morphogenetic protein (BMP) signaling.

MATERIALS AND METHODS

Generation of *Mir140*-null mice. The targeting vector was constructed to replace the 55-nucleotide sequence of the *Mir140* gene by an Flp recombinant target (FRT)-flanked neomycin-resistant gene cassette (FRT-neo) (Fig. 1A to C). The 4.4-kb-long 5′ homologous arm was PCR amplified using the high-fidelity polymerase PrimeStar (Takara-Mirus) with the primers mir140-5-5, 5′-GAGTCTGGACCTGGGTGGTTTTAG-3′, and mir140-5-3-AgeI, 5′-CACCGG TAAAACCACTGGCAGGACACAGAG-3′. The correct sequence was confirmed. The 1.9-kb-long 3′ homologous arm was similarly amplified using the primers

* Corresponding author. Mailing address: Endocrine Unit, Massachusetts General Hospital, 50 Blossom Street, Boston, MA 02114. Phone: (617) 726-3966. Fax: (617) 726-7543. E-mail: kobayash@helix.mgh.harvard.edu.

▽ Published ahead of print on 16 May 2011.

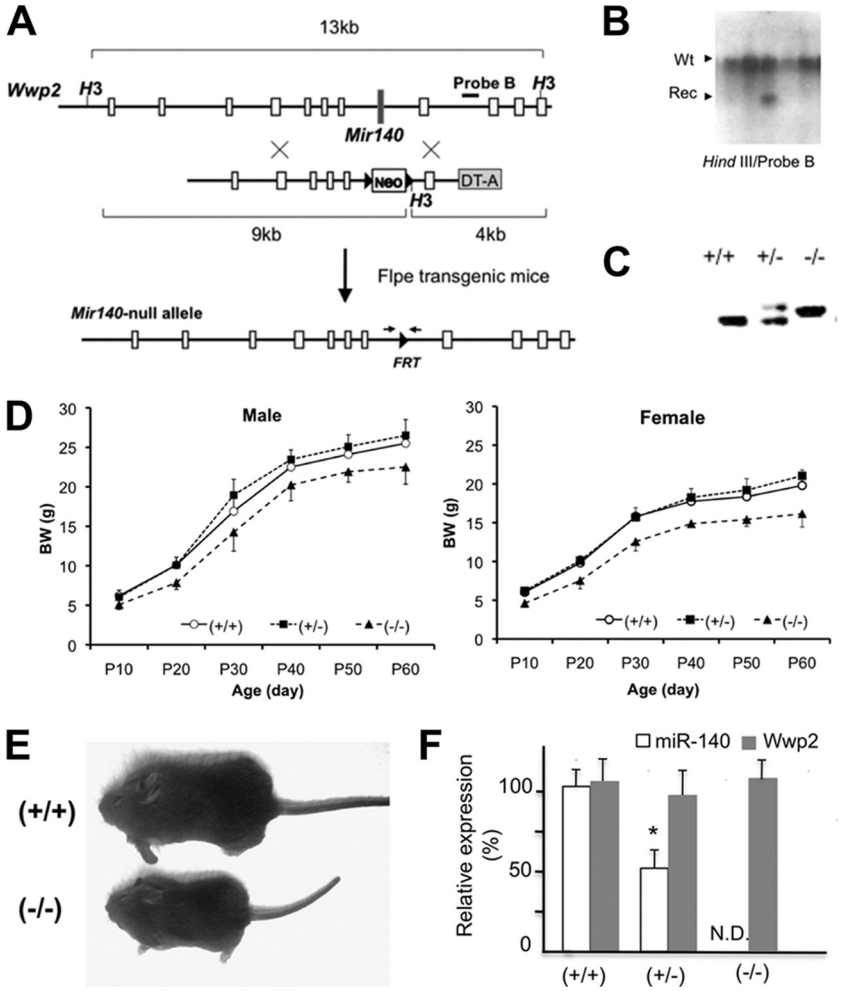

FIG. 1. Generation of *Mir140*-null mice. (A) The *Mir140* gene was replaced by an *FRT*-flanked, neomycin-resistant gene (Neo), which was subsequently removed by crossing mice with Flpe transgenic mice. (B) Southern blot analysis shows that an ES cell clone has both wild-type (Wt) and homologous recombinant (Rec) alleles. (C) PCR genotyping of mice using primers spanning *FRT* (see the small arrows in panel A). (D) *Mir140*-null mice show growth retardation in both male (left) and female (right) mice, whereas heterozygotes are indistinguishable from wild-type mice ($n > 5$). The body weight (BW) of *Mir140*-null mice was significantly lower than that of wild-type or heterozygous mice ($n = 5$; $P < 0.05$, *t* test) at all data points. (E) Picture of 3-week-old female mice. (F) miR-140 expression in primary rib chondrocytes is not detectable (N.D.) in *Mir140*-null mice, whereas miR-140 expression is reduced by approximately 50% in heterozygotes. The expression level of the host gene of *Mir140*, *Wwp2*, is not affected in *Mir140*-null mice.

mi140-3-5Spe1Hind3, 5′-ACTAGTAAGCTTACTGGAGCACCCTCTGCATC GAAG-3′, and mi140-3-3Not1, 5′-GCGGCCGCCGGCAGTGAGTAACAGTC T-3′. FRT-neo, a kind gift from Susan Dymecki, was ligated between the homologous arms. A diphtheria toxin fragment A (DT-A)-negative selectable marker was placed outside the 3′ homologous arm. The linearized targeting vector was electroporated into V6.5 embryonic stem (ES) cells (10), selected in the presence of 250 μg/ml G418. Homologous recombination was determined by Southern blot analysis and long PCR using the Phusion polymerase (New England BioLabs). ES cells carrying FRT-neo were subjected to blastocyst injection to generate chimeric mice. F1 mice carrying the mutation were further crossed to flpe transgenic mice (35) to remove FRT-neo. Mice were then backcrossed to the C57BL/6 strain for three generations. The animal experiments were approved by the Institutional Animal Care and Use Committee (IACUC) and were performed in accordance with its regulations and guidelines.

Mouse genotyping. The FRT-neo-free *Mir140*-null and wild-type alleles were detected by PCR using the primers Mi140-5S2, 5′-CTTGGTGGGCATCTGGT GTGGCTC-3′, and Mi140-3N, 5′-GAGCTAAACAATTGGGGAACAATC-3′, as 256-bp- and 233-bp-long PCR amplicons, respectively. Primer sequences to genotype *Cre* transgenic mice (19) and floxed *Pdgfra* mice (37) were described previously.

Skeletal preparation and histology. Alizarin red and Alcian blue staining was performed using a modified McLeod method (25). Carcasses were fixed in 95% ethanol, stained with Alcian blue and Alizarin red, cleared in 1% KOH, and kept in 50% glycerol. For histological analysis, mice were dissected, fixed in 10% formalin, decalcified in 10% EDTA, paraffin processed, cut, and subjected to hematoxylin-eosin staining, *in situ* hybridization, and BrdU staining. *In situ* hybridization was carried out as previously described (28). The probe for *Col10a1* was described previously (19).

BrdU labeling and detection. For BrdU labeling, 50 μg BrdU/g of body weight was given to mice intraperitoneally 2 h before sacrifice. BrdU was detected using the BrdU staining kit (Invitrogen). The BrdU labeling index was calculated as the ratio of the number of BrdU-positive nuclei over the total number of nuclei in proliferating columnar chondrocytes of the growth plate.

Primary chondrocyte isolation and culture. The frontal part of the rib cage was removed from 1.5-day-old mice, rinsed with phosphate-buffered saline (PBS), and incubated in a digestion medium containing Dulbecco modified Eagle medium (DMEM), 10% fetal calf serum (FCS), and 0.2% (approximately 600 U/ml) collagenase type II (Worthington) at room temperature for 10 min. Muscle, soft tissues, and mineralized rib and sternal bones were removed from the rib cage using fine tweezers and surgical scissors under a dissection micro-

scope. This procedure was repeated until most of the noncartilaginous tissues were removed from the specimen. Rib cartilage was further digested in fresh digestion medium at 37°C for 4 h. Cells were released from the cartilage matrix by gentle pipetting, passed through nylon mesh strainers (BD Falcon), spun to remove collagenase, counted, plated at the concentration of 5×10^5 cells/ml in the DMEM medium containing 10% FCS, and cultured overnight.

Ago2-IP and microarray analysis. Primary rib chondrocytes were cultured overnight. Total RNA was isolated from 5% of cells using SurePrep columns (Fisher) for input analysis. The rest of the cells were subjected to Ago2 immunoprecipitation (Ago2-IP) using the microRNA isolation kit Mouse Ago2 (Wako Chemicals) according to the manufacturer's instructions. For a negative control, immunoprecipitation was performed using nonimmune IgG beads prepared with the antibody immobilization bead kit (Wako Chemicals). RNA was amplified using the Ovation Pico WTA system (Nugen), labeled, and subjected to microarray analysis using HT-MG-430-PM array plates or mouse genome 430 2.0 gene chips (Affymetrix). Ago2-IP enrichment scores were calculated as normalized signal intensity ratios of total RNA and Ago2-IP RNA preparations. Genes whose Ago2-IP enrichment scores were greater than 2 were considered to be enriched in the Ago2-IP fraction.

qRT-PCR. cDNA synthesis was performed using random hexamers and the DyNAmo cDNA synthesis kit (Finnzymes). Quantitative PCR was performed using the StepOnePlus real-time PCR system (Applied Biosystems) and the EvaGreen quantitative reverse transcription-PCR (qRT-PCR) mix (Solis BioDyne). Primer sequences are as follows: GAPDH-L, 5′-CACAATTTCCATCCCAGACC-3′, and GAPDH-R, 5′-GTGGGTGCAGCGAACTTTAT-3′; Col2a1-L, 5′-AACACTTTCCAACCGCAGTC-3′, and Col2a1-R, 5′-TCTGCCCAGTTCAGGTCTCT-3′; Acan-L, 5′-GAAGAGCCTCGAATCACCTG-3′, and Acan-R, 5′-ATCCTGGGCACATTATGGAA-3′; Hmga2-L, 5′-ATCCAACTTTCTCCCCGTTC-3′, and Hmga2-R, 5′-AGGTATTGCCACAAGCAAGC-3′; Wwp2-L, 5′-ATTCTGGGCAAGGTGACAAC-3′, and Wwp2-R, 5′-GCTTTGGTCTGCTCTTCCAC-3′; Pdgfra-L, GATCCGGGCTAAGGAAGAAG-3′, and Pdgfra-R, 5′-CCAAAATGGATGCAGGAACT-3′; mouse Dnpep-L, 5′-CAGACCCTCACCCTTTTCAA-3′, and mouse Dnpep-R, 5′-TTGAAGGGGTGGAAGACAAC-3′; zebrafish Dnpep-L, 5′-CTGCGCTCATCCAGATGTTA-3′, and zebrafish Dnpep-R, 5′-GGTTGTCCAGACGAGGAGAG-3′; and zebrafish GAPDH-L, 5′-GATTGCCGTTCATCCATCTT-3′, and zebrafish GAPDH-R, 5′-GCCATCAGGTCACATACACG-3′.

Levels of expression of miR-140 and the normalization control, U6, were determined using the mirVana qRT-PCR miRNA detection kit (Ambion).

Cloning of mouse and rat *Dnpep* cDNA. Mouse *Dnpep* cDNA was PCR amplified and cloned into the pCS2+ expression vector at the EcoRI and XhoI sites using primers R1-Dnpep5, 5′-CAgaattcGCCAGTGAAGTCCTCGGAAGC-3′ and Xh-Dnpep3, 5′-CTctcgagTGAAAATCTACTTTAATAACCAACA-3′ (lowercase letters indicate attached restriction enzyme sites). Rat *Dnpep* cDNA was purchased from Open Biosystems and further subcloned into the pCS2+ vector.

Zebrafish experiments. Zebrafish maintenance and injection were performed as described previously (29). Injection of the miR-140 duplex was performed according to the protocol described previously (9).

***Mir140* binding site prediction.** The binding sites of miR-140 and miR-140* were predicted using STarMir (http://sfold.wadsworth.org/cgi-bin/starmir.pl) (7).

Transfection and luciferase assay. The predicted *Mir140*-binding sequence of Dnpep (designated BD), 5′-AACCAGGGCCTCTCGGTGCCACTGATGAGCGGCACCACTC-3′, was oligonucleotide synthesized, with the restriction enzyme sites SpeI and HindIII at its 5′ and 3′ ends, and subcloned into the pMIR-REPORT luciferase vector (Ambion). Mutant BD (5′-AACCAGGGCCTCTCGGTGggtgacATGAGCGGCtggtga3′; mutated nucleotides are shown in lowercase letters) was similarly synthesized and subcloned. One one hundredth microgram of the luciferase constructs, 0.02 μg of the *Renilla* luciferase control vector pRL-SV40, and 5 nmol of the miR-140 precursor or control (Ambion) per well of 96-well plates were cotransfected into ATDC5 cells using the Attractene transfection reagent (Qiagen). Luciferase and *Renilla* activities were measured 24 h after transfection using the dual-luciferase reporter assay system (Promega).

To assay the BMP response, the BMP reporter luciferase construct, carrying four copies of a BMP-2 responsive element in the *Id1* gene (18), and pRL-SV40 were cotransfected into BMP-responsive C2C12 cells or primary rib chondrocytes using the Attractene transfection reagent with or without a *Dnpep* expression vector or a small interfering RNA (siRNA) duplex. The sequences of the *Dnpep* siRNA duplex are 5′-CCAAUGAGGCUGAAGCCAUUGCCAGGA-3′ and 5′-CUGGCAAUGGCUUCAGCCUCAUUGG-3′. *Dnpep* siRNA and control siRNA with a scrambled sequence were purchased from Integrated DNA Technologies. Transfected cells were cultured for 24 h with or without BMP-2 (Shenandoah Biotechnology, Inc.) in 10% FCS-containing DMEM.

Western blot analysis. Anti-phospho-Smad1/5/8 antibody (Cell Signaling Technology), anti-PDGFRA antibody (Millipore), anti-Dnpep antibody (Protein Tech Group, Inc.), anti-Smad4 antibody (Genway Biotech, Inc.), and antiactin antibody (Santa Cruz Biotechnology) were purchased. Western blot analysis was performed according to the standard procedure.

Microarray data accession number. The microarray data are available in the Gene Expression Omnibus (GEO) database under the accession number GSE27177.

RESULTS

***Mir140*-null mice show defects in endochondral bone growth.** In order to investigate the physiological role of the chondrocyte-specific miRNA gene, *Mir140*, mice lacking *Mir140* were generated by gene targeting (Fig. 1A to C). *Mir140*-null mice survived postnatally and reached adulthood but showed impaired growth (Fig. 1D and E). The *Mir140* gene is present in an intron of the *Wwp2* gene, which encodes an E3 ubiquitin ligase. The deletion of the *Mir140* gene did not alter the expression level of *Wwp2* in primary chondrocytes, whereas miR-140 miRNA was not detectable in *Mir140*-null mice (Fig. 1F).

As suggested by the postnatal growth retardation of *Mir140*-null mice, long bones, which grow through endochondral bone formation, were significantly shorter in *Mir140*-null mice than in control mice (Fig. 2A and B). Another characteristic skeletal phenotype of *Mir140*-null mice was a defect in the longitudinal growth of the skull (Fig. 2C and D). Like long bones, longitudinal growth of the basal skull is mediated primarily by the growth plate cartilage. The shortening of these bones in the basal skull was detectable even in embryonic stages (Fig. 2E). A sagittal section of the basisphenoidal bone, flanked by bidirectional growth plates, at postnatal day 5.5 (P5.5) showed a reduction in longitudinal length (Fig. 2F).

***Mir140* deficiency results in mild acceleration of chondrocyte differentiation and bone development.** As in endochondral bones of the skull, mild skeletal abnormalities were observed in endochondral bones in other parts of the body at embryonic and neonatal stages. At birth, we found that talus bone development was consistently advanced in *Mir140*-null mice, as indicated by its large mineralized area (Fig. 3A and B). Similarly, the initial mineralization of the radius, ulna at embryonic day 14.5 (E14.5), and the hyoid horn at P1.5 was advanced in *Mir140*-null mice (Fig. 3C and see Fig. 5D). *In situ* hybridization to detect *Col10a1*, a specific marker of hypertrophic chondrocytes, indicated an increase in the size of the hypertrophic region of the talus at P0.5 and tibia at E14.5 in *Mir140*-null mice (Fig. 3D and E). The size of the hypertrophic region of the tibia was significantly larger in *Mir140*-null mice (0.473 ± 0.003 mm versus 0.503 ± 0.008 mm) ($n = 3$ each; $P < 0.05$, t test) than in normal mice. These findings suggest that initial hypertrophic differentiation and subsequent bone formation occur prematurely in the absence of *Mir140*.

Premature differentiation of proliferating chondrocytes into postmitotic hypertrophic chondrocytes causes shortening of bones by reducing the number of proliferating chondrocytes, as exemplified by mutant mice lacking parathyroid hormone-related peptide (PTHrP) signaling, a pivotal regulator of chondrocyte differentiation (16, 22). It is therefore possible that mild acceleration of differentiation into postmitotic hypertrophic chondrocytes reduced the net mass of growth plate chon-

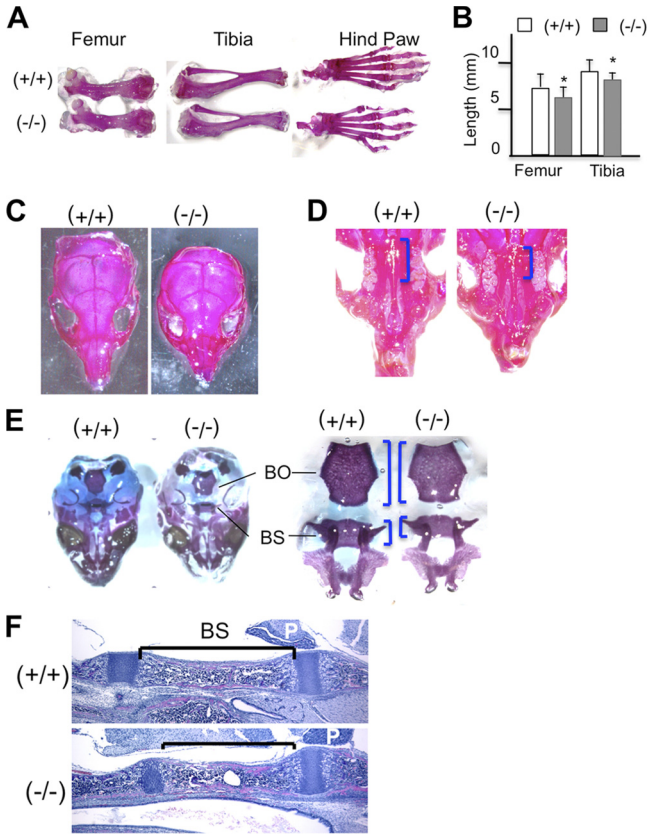

FIG. 2. The longitudinal growth of endochondral bones is impaired in *Mir140*-null mice. Whole-mount Alizarin staining (A to D) shows the shortening of the indicated long bones (A), skull (C), and palate (D) of a 4-week-old male *Mir140*-null mouse. Brackets indicate palatal bones. (B) The lengths of the femur and tibia of 2-week-old *Mir140*-null mice are significantly smaller than those of wild-type littermates ($n = 3$; $P < 0.05$, t test). (E) Alizarin staining shows mild shortening of bones of the basal skull (right) of E17.5 *Mir140*-null embryos. BO, basioccipital bone; BS, basisphenoidal bone. (F) Hematoxylin and eosin-stained sections of the basisphenoidal bone (BS) of 5.5-day-old mice. The basisphenoidal bone (brackets) is shortened in *Mir140*-null mice. The bidirectional growth plates flanking this bone are slightly shortened. P, pituitary gland.

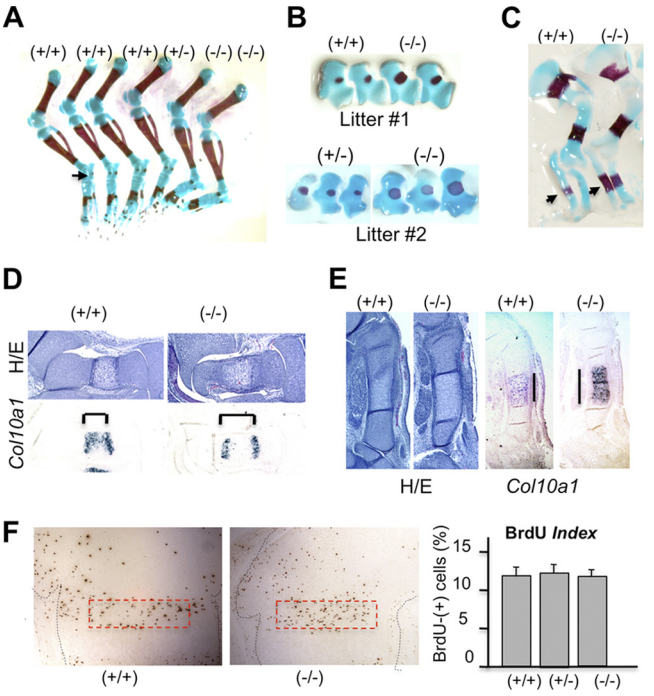

FIG. 3. Mild acceleration of bone development in *Mir140*-null mice. Whole-mount skeletal staining (A to C) shows an advanced mineralization of the talus (arrow) in newborn *Mir140*-null hind limbs (A). The sizes of Alizarin red-stained mineralized areas of the talus (B) and forearms (C) are greater in *Mir140*-null mice than in wild-type or heterozygous littermates. Arrows indicate mineralization of the ulna. (D, E) The size of the hypertrophic region marked by *Col10a1* (brackets) is greater in the talus at P0.5 (D) and the tibia at E14.5 (E) than in control animals, suggesting accelerated hypertrophic differentiation of chondrocytes. Brackets and black lines indicate the hypertrophic region. H/E, hematoxylin and eosin stain. (F) Growth plates of the *Mir140*-null tibia at P5.5 exhibit no significant proliferation defects in proliferating columnar chondrocytes.

drocytes over time, leading to the growth defects observed in *Mir140*-null mice.

We did not find an alteration in the proliferation of columnar chondrocytes in *Mir140*-deficient tibiae at P5.5 (Fig. 3F), P21, P14, P3.5, or E17.5 (data not shown). These results suggest that impairment of endochondral bone growth in *Mir140*-null mice is caused primarily by altered chondrocyte differentiation.

Reciprocal change in the sizes of the resting and columnar zones in the *Mir140*-null growth plate. In growth plates, chondrocytes in the resting zone proliferate slowly and then differentiate into vigorously proliferating columnar chondrocytes. Changes in cellular differentiation at this step influence the columnar length (21). Chondrocytes in the resting zone are small and do not form distinct columns, whereas columnar chondrocytes are flat and form orderly columns.

The growth plate morphology at early postnatal stages was relatively normal (data not shown). However, at later stages, when the secondary ossification center is already formed, we found that *Mir140*-null growth plates showed an increase in the size of the resting zone and a modest decrease in the size of the columnar zone (Fig. 4A to C). This finding suggests a possible inhibition of chondrocyte differentiation from the resting zone into proliferating columnar chondrocytes. We did not find significant shortening of the overall growth plate length in *Mir140*-null mice.

***Pdgfra* is not a physiologically important target of *Mir140* in mouse skeletal development.** It has been shown that miR-140 targets *Pdgfra* to control palatal skeletogenesis in zebrafish (9). Since *Pdgfra* is also predicted to be a miR-140 target in mice, we tested whether PDGFRA expression was altered in mouse chondrocytes lacking *Mir140*. We did not find upregulation of PDGFRA expression in *Mir140*-null primary rib chondrocytes (Fig. 5A), in contrast to results for zebrafish with the miR-140 knockdown. In order to examine the possible causal role of the loss of *Mir140*-dependent *Pdgfra* suppression in the skeletal defect of *Mir140*-null mice, we tested whether genetic deletion of *Pdgfra* in chondrocytes could rescue the skeletal defect of *Mir140*-null mice. The *Pdgfra* gene was ablated in chondrocytes using the Cre-*loxP* binary system; Cre mice expressing Cre in chondrocytes under the control of a type II collagen promoter

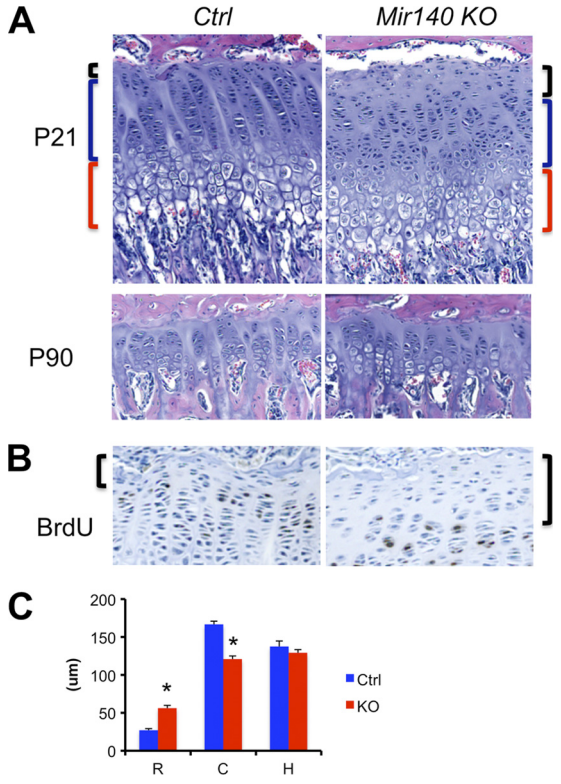

FIG. 4. (A) Reciprocal change in the sizes of the resting and columnar zones of the *Mir140*-null growth plate. Hematoxylin and eosin-stained growth plates of the proximal tibia at P21 show an increase in the size of the resting zone (black brackets) and a modest decrease in the size of the columnar zone (blue brackets) in *Mir140*-null mice (KO) compared with those of control mice (Ctrl). This tendency is present but less appreciable in older mice (P90). (B) The resting zone (brackets), containing chondrocytes with low BrdU incorporation rates, is expanded in the *Mir140*-null growth plate. (C) The length of each layer was measured in 21-day-old control (wild-type and heterozygous mice) and *Mir140*-null littermates. The columnar zone (bars labeled C) was defined as the region containing columns formed by more than 5 chondrocytes per column. The resting (bars R) and hypertrophic (bars H) zones are defined as the cartilage area adjacent to the columnar zone (*, $P < 0.05$, $n = 3$, t test).

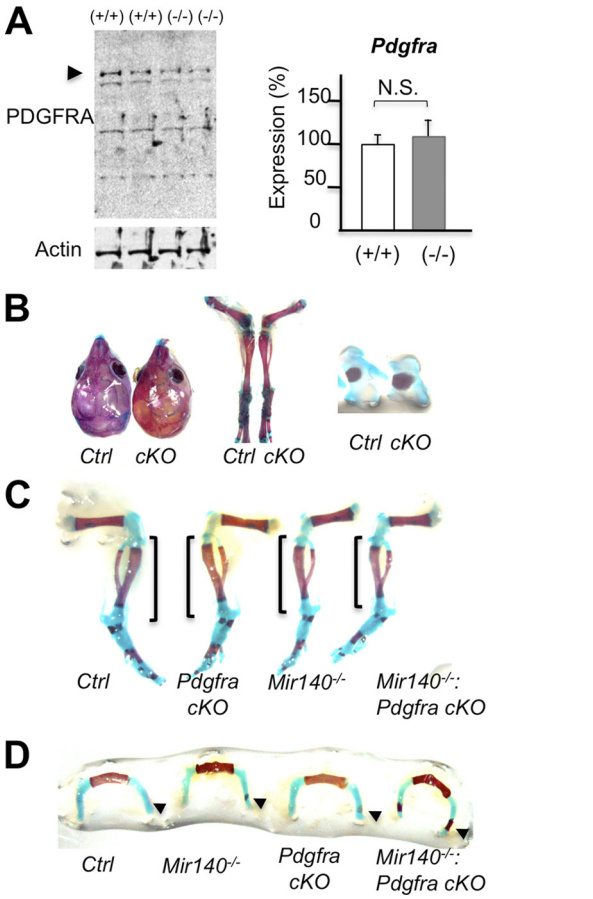

FIG. 5. PDGFRA is not a physiologically important target of *Mir140* in mouse chondrocytes. (A) PDGFRA expression is not up-regulated in *Mir140*-null primary chondrocytes. Multiple bands detected by immunoblot analysis using anti-PDGFRA antibody in primary rib chondrocytes (left). The top two bands (arrowhead) migrate at the expected molecular masses (150 and 170 kDa). *Pdgfra* mRNA expression determined by qRT-PCR was not significantly altered in *Mir140*-null primary chondrocytes. N.S., not significant. (B) A chondrocyte-specific PDGFRA knockout (cKO) shows mild shortening of the longitudinal length of the skull and long bones. Skeletal preparation of the skull (left) and hind limbs (middle) at P10.5. Mineralization of the talus at P0.5 is slightly advanced in cKO mice (right). (C, D) Conditional ablation of *Pdgfra* does not rescue the skeletal defect of *Mir140*-null mice. (C) At P1.5, the shortening of the long bones of *Mir140*-null mice is not rescued by conditional *Pdgfra* ablation in chondrocytes. (D) The advanced mineralization of the hyoid horns (arrowheads) of 1.5-day-old *Mir140*-null mice was even augmented but not rescued in doubly mutant mice.

(32) were crossed to floxed *Pdgfra* (*Pdgfra*$^{fl/fl}$) mice (37). Heterozygous conditional *Pdgfra*-null (*Cre Pdgfra*$^{fl/+}$) and compound heterozygous (*Cre Pdgfra*$^{fl/+}$ *Mir140*$^{+/-}$) mice were indistinguishable from wild-type littermates. These mice were further crossed with *Mir140*-null mice to generate compound homozygous mutants (*Cre Pdgfra*$^{fl/fl}$ *Mir140*$^{-/-}$). In the genetic background used in this study, chondrocyte-specific *Pdgfra*-deficient mice (conditional knockout [cKO]) survived postnatally and reached adulthood. However, *Pdgfra* cKO mice showed a mild reduction in growth. The body weight of *Pdgfra* cKO mice at P28 was about 10% less than that of control littermates (11.5 ± 0.4 g versus 13.2 ± 0.3 g), but the mice showed grossly normal appearance. Despite the mild reduction in size, mineralization of the talus at P0.5 was slightly greater in cKO mice and similar to that of *Mir140*-null mice (Fig. 5B). *Mir140*-null *Pdgfra* cKO doubly mutant mice were slightly smaller and had slightly shorter long bones than *Mir140*-null littermates, demonstrating that *Pdgfra* ablation was unable to rescue the defect in the long bone growth of *Mir140*-null mice (Fig. 5C). At P1.5, the hyoid horn of *Mir140*-null mice showed advanced mineralization similar to that of the talus, ulna, and radius at earlier stages. Again, simultaneous ablation of *Pdgfra* did not rescue the advanced hyoid mineralization (Fig. 5D). These results indicate that *Pdgfra* is not a physiologically important target of *Mir140* in mouse chondrocytes.

***Mir140* targets *Dnpep*.** To understand the molecular mechanism by which *Mir140* regulates endochondral bone development, we sought to identify target transcripts of *Mir140* miRNAs. We took advantage of the finding that RNA immunoprecipitation using anti-Argonaute (Ago) antibodies can iden-

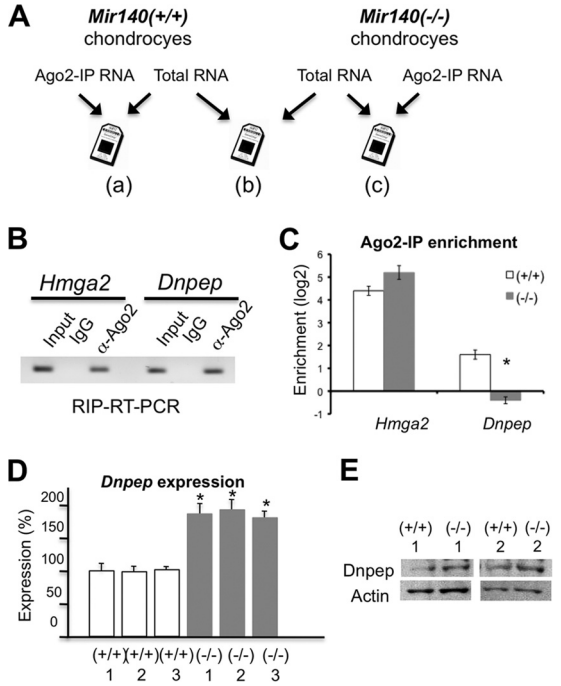

FIG. 6. miR-140 targets *Dnpep* in mouse chondrocytes. (A) Experimental strategy. RNA was prepared from the Ago2-IP fraction and total RNA from wild-type and *Mir140*-null primary chondrocytes and subjected to expression profiling. RNA enriched in the Ago2-IP fraction was first identified in wild-type (a) and *Mir140*-null (c) chondrocytes; genes that were enriched in the Ago2-IP fraction in wild-type but not in *Mir140*-null chondrocytes were selected. Among them, those upregulated in *Mir140*-null chondrocytes (b) were subjected to further investigation. (B) RNA immunoprecipitation followed by RT-PCR (RIP-RT-PCR) shows the specific association between *Hmga2* and *Dnpep* transcripts and Ago2 in wild-type cells. (C) *Dnpep* is associated with Argonaute 2 (Ago2) in wild-type but not in *Mir140*-null chondrocytes. Ago2 association was determined by comparing transcript levels of Ago2 immunoprecipitants with those of total RNA (Input in panel B). Transcript levels were expressed relative to that of *GAPDH* of each fraction. Ago2-IP enrichment ratios were calculated by dividing normalized transcript levels in the Ago2-IP RNA by those in total RNA. The relative enrichment of *Dnpep* in the Ago2-IP fraction is significantly less in *Mir140*-null chondrocytes, whereas *Hmga2*, a quintessential target of *let-7* miRNAs, is enriched in the Ago2-IP fractions of both *Mir140*-null and wild-type chondrocytes ($*$, $P < 0.05$, $n = 4$, t test). (D, E) Dnpep is upregulated in *Mir140*-null primary rib chondrocytes both at the RNA level (D) and at the protein level (E).

tify miRNA-regulated genes (4, 8, 12, 13, 17, 42). We reasoned that (i) Ago-associated RNAs in wild-type chondrocytes should contain *Mir140* targets, (ii) RNAs that are regulated predominantly by *Mir140* should be associated with Ago to a lesser extent in *Mir140*-null than in wild-type chondrocytes, and (iii) genes regulated mainly by *Mir140* should be upregulated in *Mir140*-null chondrocytes, since miRNA-RNA interaction usually leads to RNA degradation (11). We performed immunoprecipitation using an antibody against Argonaute 2, the most abundant Ago in mice (Ago2-IP). In wild-type chondrocytes, the well-known *let-7* miRNA target transcript *Hmga2* (23, 24), along with *Dnpep*, was immunoprecipitated with this antibody but not nonimmune IgG (Fig. 6B). We profiled Ago2-associated transcripts by microarray analysis and screened them according to the screening strategy depicted (Fig. 6A). We examined genes with relatively high signal intensities by quantitative reverse transcription-PCR (qRT-PCR) and confirmed that the gene encoding an aspartyl aminopeptidase, *Dnpep*, was enriched in the Ago2-IP fraction of wild-type but not *Mir140*-null chondrocytes (Fig. 6C). On the other hand, *Hmga2* was similarly enriched in the Ago2-IP fractions of both wild-type and *Mir140*-null chondrocytes. As expected, *Dnpep* expression was upregulated in *Mir140*-null chondrocytes (Fig. 6D and E). To further confirm the interaction between miR-140 and *Dnpep*, we coinjected a miR-140 duplex and *Dnpep* mRNA into zebrafish embryos. Injection of miR-140 causes defects in palatal skeletogenesis in zebrafish (9). Coinjection of mouse *Dnpep* mRNA significantly reduced the occurrence of the miR-140-induced palatal defect (Fig. 7A). Interestingly, coinjection of rat *Dnpep* mRNA also had the same effect. Zebrafish *Dnpep* lacks strongly predicted miR-140 binding sites, and expression of endogenous zebrafish *Dnpep* was unchanged 1 and 3 days after miR-140 injection (data not shown), suggesting that miR-140 does not regulate zebrafish *Dnpep*; therefore, this rescue likely occurred because coinjected *Dnpep* sequesters miR-140. This result suggests a direct interaction between miR-140 and *Dnpep* transcripts. Bioinformatics analysis using STarMir (7) identified multiple potential binding sites of miR-140 in the full mouse and rat *Dnpep* sequence. However, only a single site located in the coding sequence was commonly predicted in mouse and rat *Dnpep.* This site is located in a 45-nucleotide-long region (designated BD) that contained two potential miR-140 binding sites in mouse *Dnpep* (Fig. 7B). To test whether the BD sequence could mediate the miR-140–*Dnpep* interaction, a luciferase reporter plasmid carrying the BD sequence was constructed. Cotransfection with a miR-140 miRNA precursor reduced the luciferase activity of the reporter construct with the BD but not a mutated BD sequence, suggesting that miR-140 suppresses *Dnpep* expression by binding to BD (Fig. 7C). Furthermore, transfection of the miR-140 precursor into chondrogenic ATDC5 cells reduced Dnpep expression (Fig. 7D).

Dnpep antagonizes BMP signaling downstream of Smad activation. Dnpep has been suggested to be involved in intracellular peptide metabolism, but its role *in vivo* is not known. In order to understand the possible role of *Dnpep in vivo*, first, we overexpressed *Dnpep* in zebrafish embryos. The majority of the injected embryos showed grossly normal development. However, we found that 4.2 to 6.3% of *Dnpep*-injected embryos showed dorsalization, whereas dorsalization was never observed in green fluorescent protein (GFP)-injected embryos (Fig. 8A and B). Dorso-ventral patterning in zebrafish embryos is controlled by BMP and Wnt signaling (36). Since dorsalized, *Dnpep*-injected embryos maintained anterior head structures, whose formation is antagonized by Wnt signaling, we speculated that dorsalization caused by *Dnpep* overexpression was due to reduced BMP signaling, rather than increased Wnt signaling. To test this possibility, we coinjected *Bmp2b* and *Dnpep* into zebrafish embryos to test whether *Dnpep* could antagonize the ventralization effect caused by *Bmp2b* overexpression (Fig. 8C and D). *Dnpep* coinjection caused a mild but significant inhibitory effect in the ventralization induced by *Bmp2b*. This result further supports the antagonistic effect of Dnpep in BMP signaling. In order to test whether this effect is conserved in mammalian cells, we overexpressed *Dnpep* along

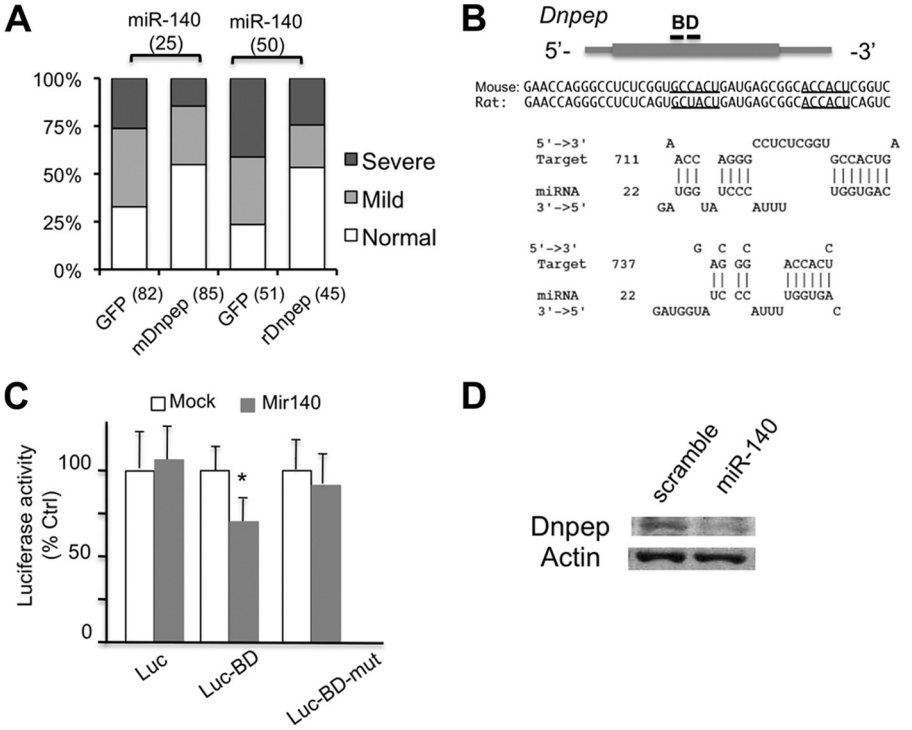

FIG. 7. Direct interaction between miR-140 and *Dnpep* suppresses *Dnpep* expression. (A) Coinjection of mouse or rat *Dnpep* rescues miR-140-induced palatal defects in zebrafish. Zebrafish embryos were injected with 3 nl of 25 μM miR-140 or 50 μg of miR-140 duplex solution with 1 ng of the indicated synthesized mRNA. The total numbers of analyzed fish are indicated in parentheses below the graph. The severity of the skeletal phenotypes was judged according to the criteria described previously (9). Fractions of fish with normal development were significantly greater in mouse or rat *Dnpep*-coinjected animals than in control animals ($P < 0.05$, χ^2 test). (B) A major miR-140 binding site (BD) and its sequence predicted by STarMir are shown. The coding and untranslated regions are indicated by a gray box and lines, respectively. Underlines indicate seed sequence binding sites. (C) A luciferase reporter construct carrying the 45-nucleotide-long BD sequence, but not a mutated BD, shows a reduction in luciferase activity upon miR-140 cotransfection. The luciferase activity was normalized to that of cotransfected *Renilla* luciferase. (*, $P < 0.05$, $n = 4$, t test). (D) miR-140 transfection into ATDC5 cells reduces Dnpep expression.

with a BMP reporter construct carrying the BMP-responsive element of the *Id1* gene (18). *Dnpep* overexpression in BMP-responsive C2C12 cells showed significantly reduced responses to BMP-2 (Fig. 9A). Since *Dnpep* was upregulated in *Mir140*-null chondrocytes, we tested the BMP activity of *Mir140*-null primary rib chondrocytes. Primary rib chondrocytes were transfected with the BMP reporter construct and treated with BMP-2. We found that the reporter activity was consistently lower in *Mir140*-null chondrocytes than in the control (Fig. 9B) at any BMP concentration. However, upon stimulation with BMP-2, the reporter activity increased in a dose-dependent manner in both control and *Mir140*-null chondrocytes. *Mir140*-null chondrocytes showed a normal response in the phosphorylation of Smad1/5/8 upon BMP treatment, an immediate consequence of BMP receptor activation, and a normal level of the Smad1/5/8 binding partner, Smad4 (Fig. 9C and D). These results suggest that BMP-dependent gene transcription is compromised in *Mir140*-null chondrocytes at a position downstream of Smad activation. Next, we tested whether overexpression of *Dnpep* reduces the BMP reporter activity in primary chondrocytes. Primary chondrocytes were cotransfected with reporter constructs and a *Dnpep* expression vector and cultured in the presence of 50 ng/ml of BMP-2. *Dnpep* overexpression reduced the basal BMP reporter activity both in control and in *Mir140*-null chondrocytes (Fig. 9E). Conversely, *Dnpep* knockdown using siRNA increased BMP reporter activity in *Mir140*-null chondrocytes (Fig. 9F). These results show that *Dnpep* upregulation negatively regulates BMP signaling in *Mir140*-null chondrocytes.

DISCUSSION

We have shown that loss of the chondrocyte-specific miRNA gene, *Mir140*, in mice causes defects in endochondral bone development. Since there were no overt changes in the proliferation of *Mir140*-null growth plate chondrocytes, the growth defects observed in *Mir140*-null mice are likely caused by the acceleration of chondrocyte differentiation into postmitotic hypertrophic chondrocytes. Although the acceleration of hypertrophic differentiation is relatively mild, causing few detectable histological changes, it is possible that, over time, these defects negatively influence the production of the net chondrocyte mass, leading to a visible reduction in the skeletal size of *Mir140*-null mice. A recent study describing separately generated *Mir140*-null mice reports a reduction in the proliferation and shortening of the growth plates (27). In this study, we did not find significant reductions in chondrocyte proliferation or growth plate length at multiple stages of development. The reason for these disparities is not clear. We backcrossed mice to the C57BL/6 strain for three generations, and it is possible

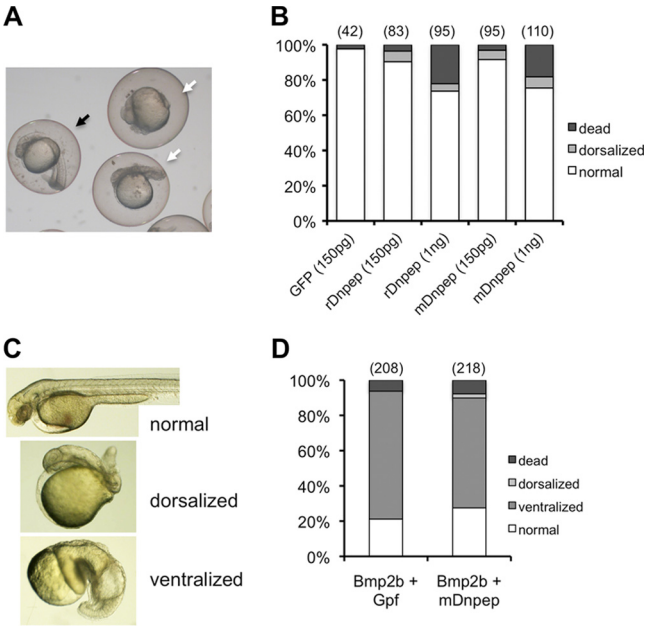

FIG. 8. Negative regulation of BMP activity by Dnpep. (A, B) Dorsalization in zebrafish overexpressing *Dnpep*. (A) Representative picture of dorsalized (white arrows) and normal (black arrow) embryos. Shortening of the tail and preservation of anterior structures of the head are observed at 30 h postfertilization. (B) About 4 to 6% of Dnpep-injected zebrafish show dorsalization ($P < 0.05$, χ^2 test). The number of injected embryos per experimental group is indicated in parentheses above the graph. (C, D) *Dnpep* coinjection reduces the occurrence of ventralization caused by Bmp2b ($P < 0.05$, χ^2 test). Numbers of injected animals are indicated in parentheses. Pictures were taken at 30 to 35 h postfertilization.

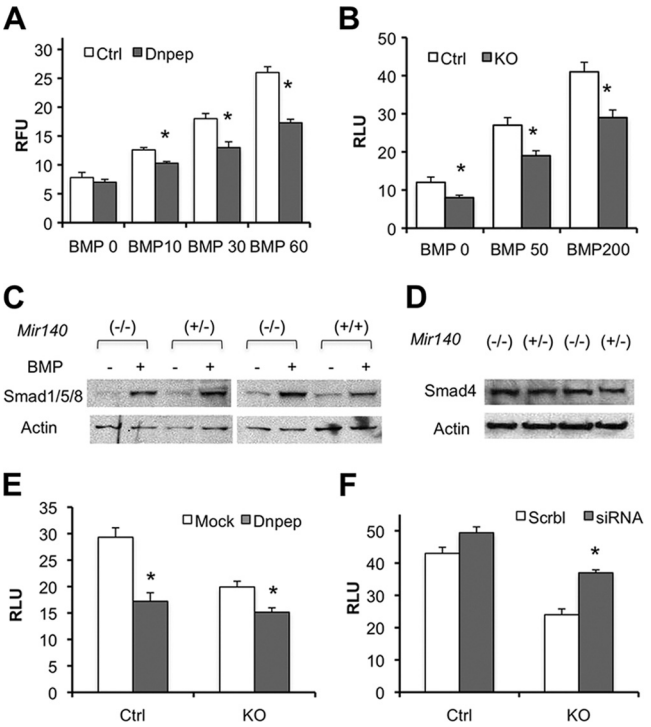

FIG. 9. Dnpep dampens BMP signaling in mammalian cells. (A) BMP-responsive C2C12 cells were cotransfected with a BMP-responsive luciferase reporter (Id1-Luc), a *Renilla* luciferase (pRL-SV40) control, and an empty (control) or a *Dnpep* expression vector. Cells were treated with BMP-2 at the indicated concentrations (ng/ml) for 24 h. Relative luciferase activity normalized by that of *Renilla* luciferase was significantly reduced in *Dnpep*-overexpressing cells. (*, $P < 0.05$, $n = 5$, t test). RLU, relative light units. (B) Reduced BMP reporter activity in *Mir140*-null chondrocytes. Primary rib chondrocytes were transfected with Id1-Luc and treated with BMP-2 at the indicated concentrations for 24 h. *Mir140*-null chondrocytes show significantly lower normalized luciferase activities than those of the control (*, $P < 0.05$, $n = 8$, t test). (C, D) Smad phosphorylation (C) or the Smad4 level (D) is not affected in *Mir140* deficiency. (E) *Dnpep* overexpression significantly reduced BMP reporter activity both in control and in *Mir140*-null (KO) chondrocytes (*, $P < 0.05$, $n = 8$, t test). Cells were cultured in the presence of 50 ng/ml of BMP-2 for 24 h. (F) An siRNA-mediated knockdown of *Dnpep* increased BMP reporter activity. siRNA duplexes were cotransfected to primary rib chondrocytes with Id1-Luc and pRL-SV40. Cells were cultured in the presence of 50 ng/ml of BMP-2 for 24 h. The *Dnpep* siRNA significantly increased the BMP reporter activity in *Mir140*-null chondrocytes (*, $P < 0.05$, $n = 6$, t test).

that the difference in the genetic background may influence the phenotype. We found a relative increase in the size of the resting zone and a mild decrease in the size of the columnar zone in 3-week-old *Mir140*-null mice. This finding suggests a possible inhibition of resting chondrocyte differentiation into columnar chondrocytes. Stimulation of chondrocyte differentiation at this step increases the length of the columnar zone (21). Therefore, it is likely that inhibition of this step would cause a reduction in proliferating columnar chondrocytes. As with acceleration of hypertrophic differentiation, inhibition of this step would also decrease the number of proliferating chondrocytes, resulting in the shortening of endochondral bones.

The skeletal abnormalities of *Mir140*-null mice differ from those reported in zebrafish with a miR-140 knockdown (9). Mice lacking *Mir140* show a shortening of the palate rather than the elongation observed in zebrafish with miR-140 knocked down. The zebrafish study demonstrated that miR-140 suppressed the expression of PDGFRA, which regulates the migration of neural crest-derived mesenchymal cells to the rostral region. Although *Pdgfra* is also predicted to be a target of miR-140 in mice, we did not find significant alterations in PDGFRA expression in *Mir140*-null chondrocytes. In addition, genetic ablation of *Pdgfra* did not lessen the skeletal defect of *Mir140*-null mice. These data demonstrate that, unlike in zebrafish palatal development, *Pdgfra* is not a physiologically important target in mouse chondrocytes. This finding underscores the possibility that a miRNA may have substantially different sets of target transcripts and thus may play different physiological roles, dependent on animal species and cell types.

Identification of miRNA targets has been a challenge. Bioinformatics approaches have offered only limited solutions. Since bioinformatics approaches rely solely on base pairing of miRNAs and target RNAs, they do not take into account particular cellular contexts, such as expression levels of target RNAs and miRNAs. Therefore, to identify physiologically meaningful targets of miRNAs, it is necessary to experimentally examine miRNA-RNA interactions under specific conditions. A few methods have been developed to experimentally identify miRNA targets. Based on the fact that miRNAs bind to target RNAs through base pairing, miRNA-target RNA complexes were successfully isolated by pulldown assays

using biotin- or digoxigenin-tagged miRNAs (15, 31). However, these methods may not reveal physiologically relevant interactions because tagged RNAs need to be exogenously added. In this study, we performed RNA immunoprecipitation using anti-Ago2 antibody (Ago2-IP) to isolate RNAs regulated by endogenous miRNAs in chondrocytes. Since *Mir140* is one of the most abundant miRNAs in chondrocytes, we reasoned that *Mir140* target RNAs should be enriched in the Ago2-IP fraction along with targets of other miRNAs expressed in chondrocytes and, therefore, that comparing profiles of Ago2-associated RNA between wild-type and *Mir140*-null chondrocytes would reveal target transcripts regulated mainly by *Mir140*. We found only 44 genes (data not shown), including *Dnpep*, that satisfied the screening criteria. Since many RNAs can be regulated by multiple miRNAs, it is likely that this strategy can identify only RNAs whose expression is regulated exclusively by *Mir140*. This screening did not find previously reported targets of miR-140, such as *Pdgfra* (9), *Adamts5* (27), *Hdac4* (38), or *CxCl12* (30). It is possible that these genes may also be regulated by other miRNAs, and therefore, loss of miR-140 alone does not significantly reduce the interaction with Ago2.

Coinjection of both mouse and rat *Dnpep* transcripts suppressed the miR-140-induced palatal defect in zebrafish, but the only commonly predicted binding sequence was found in the coding sequence. It has been increasingly appreciated that miRNAs bind sequences beyond the 3′ untranslated region of genes (6). Since this short sequence was able to reduce reporter activity in a miR-140-dependent manner, it is likely that *Dnpep* expression is regulated by miR-140, at least in part, through this sequence.

Dnpep encodes an aspartyl aminopeptidase that catalyzes the sequential removal of amino acids from the unblocked N termini of peptides and proteins. Although *Dnpep* is expressed broadly, its physiological role in mammalian cells is poorly understood. It is speculated that aspartyl aminopeptidases are involved in protein and peptide metabolism and possibly in modulation of biologically active peptides such as angiotensin I (2). *Dnpep* overexpression in this study suggested that *Dnpep* had a weak antagonistic effect on BMP signaling. We found that the BMP reporter activity in *Mir140*-null chondrocytes was significantly reduced and that manipulation of *Dnpep* in primary chondrocytes confirmed that Dnpep negatively regulated the BMP reporter activity. *In vivo* reporter analysis has demonstrated a robust BMP-dependent transcriptional activity in growth plate chondrocytes (5). BMP signaling regulates cartilage development at multiple steps; it is essential for early chondrocyte differentiation (34, 41) and for maintaining the mass of proliferating chondrocytes by antagonizing fibroblast growth factor (FGF) signaling (26). Therefore, it is possible that the reduced BMP action in chondrocytes contributes to the skeletal defects of *Mir140*-null mice.

The mechanism by which *Dnpep* antagonizes BMP signaling is not clear at the moment. Smad phosphorylation and the Smad4 level in *Mir140*-null chondrocytes were unaffected. Although the BMP reporter activity in *Mir140*-null chondrocytes is constantly reduced compared with that in the control, *Mir140*-null chondrocytes respond reasonably well to exogenous BMP-2. These data suggest that Dnpep inhibits BMP action at a position downstream of Smad activation. For example, Dnpep might degrade cofactors of Smads in the regulation of gene transcription.

ACKNOWLEDGMENTS

We thank the MGH Transgenic Core Facility for blastocyst injection. We thank the BIDMC Genomics and Proteomics Center for microarray analysis.

This work was supported by the National Institutes of Health (grants AR054500 and AR056645 to T.K.) and the American Society for Bone and Mineral Research (grant CEA0811 to T.K.).

REFERENCES

1. **Ambros, V., and X. Chen.** 2007. The regulation of genes and genomes by small RNAs. Development **134:**1635–1641.
2. **Banegas, I., et al.** 2006. Brain aminopeptidases and hypertension. J. Renin Angiotensin Aldosterone Syst. **7:**129–134.
3. **Bartel, D. P.** 2009. MicroRNAs: target recognition and regulatory functions. Cell **136:**215–233.
4. **Beitzinger, M., L. Peters, J. Y. Zhu, E. Kremmer, and G. Meister.** 2007. Identification of human microRNA targets from isolated argonaute protein complexes. RNA Biol. **4:**76–84.
5. **Blank, U., et al.** 2008. An *in vivo* reporter of BMP signaling in organogenesis reveals targets in the developing kidney. BMC Dev. Biol. **8:**86.
6. **Brodersen, P., and O. Voinnet.** 2009. Revisiting the principles of microRNA target recognition and mode of action. Nat. Rev. Mol. Cell Biol. **10:**141–148.
7. **Ding, Y., C. Y. Chan, and C. E. Lawrence.** 2005. RNA secondary structure prediction by centroids in a Boltzmann weighted ensemble. RNA **11:**1157–1166.
8. **Easow, G., A. A. Teleman, and S. M. Cohen.** 2007. Isolation of microRNA targets by miRNP immunopurification. RNA **13:**1198–1204.
9. **Eberhart, J. K., et al.** 2008. MicroRNA Mirn140 modulates Pdgf signaling during palatogenesis. Nat. Genet. **40:**290–298.
10. **Eggan, K., et al.** 2001. Hybrid vigor, fetal overgrowth, and viability of mice derived by nuclear cloning and tetraploid embryo complementation. Proc. Natl. Acad. Sci. U. S. A. **98:**6209–6214.
11. **Guo, H., N. T. Ingolia, J. S. Weissman, and D. P. Bartel.** 2010. Mammalian microRNAs predominantly act to decrease target mRNA levels. Nature **466:**835–840.
12. **Hayashida, Y., T. Nishibu, K. Inoue, and T. Kurokawa.** 2009. A useful approach to total analysis of RISC-associated RNA. BMC Res. Notes **2:**169.
13. **Hendrickson, D. G., D. J. Hogan, D. Herschlag, J. E. Ferrell, and P. O. Brown.** 2008. Systematic identification of mRNAs recruited to argonaute 2 by specific microRNAs and corresponding changes in transcript abundance. PLoS One **3:**e2126.
14. **Hornstein, E., and N. Shomron.** 2006. Canalization of development by microRNAs. Nat. Genet. **38**(Suppl.)**:**S20–S24.
15. **Hsu, R. J., H. J. Yang, and H. J. Tsai.** 2009. Labeled microRNA pull-down assay system: an experimental approach for high-throughput identification of microRNA-target mRNAs. Nucleic Acids Res. **37:**e77.
16. **Karaplis, A. C., et al.** 1994. Lethal skeletal dysplasia from targeted disruption of the parathyroid hormone-related peptide gene. Genes Dev. **8:**277–289.
17. **Karginov, F. V., et al.** 2007. A biochemical approach to identifying microRNA targets. Proc. Natl. Acad. Sci. U. S. A. **104:**19291–19296.
18. **Katagiri, T., et al.** 2002. Identification of a BMP-responsive element in Id1, the gene for inhibition of myogenesis. Genes Cells **7:**949–960.
19. **Kobayashi, T., et al.** 2002. PTHrP and Indian hedgehog control differentiation of growth plate chondrocytes at multiple steps. Development **129:**2977–2986.
20. **Kobayashi, T., et al.** 2008. Dicer-dependent pathways regulate chondrocyte proliferation and differentiation. Proc. Natl. Acad. Sci. U. S. A. **105:**1949–1954.
21. **Kobayashi, T., et al.** 2005. Indian hedgehog stimulates periarticular chondrocyte differentiation to regulate growth plate length independently of PTHrP. J. Clin. Invest. **115:**1734–1742.
22. **Lanske, B., et al.** 1996. PTH/PTHrP receptor in early development and Indian hedgehog-regulated bone growth. Science **273:**663–666.
23. **Lee, Y. S., and A. Dutta.** 2007. The tumor suppressor microRNA let-7 represses the HMGA2 oncogene. Genes Dev. **21:**1025–1030.
24. **Mayr, C., M. T. Hemann, and D. P. Bartel.** 2007. Disrupting the pairing between let-7 and Hmga2 enhances oncogenic transformation. Science **315:**1576–1579.
25. **McLeod, M. J.** 1980. Differential staining of cartilage and bone in whole mouse fetuses by alcian blue and alizarin red S. Teratology **22:**299–301.
26. **Minina, E., C. Kreschel, M. C. Naski, D. M. Ornitz, and A. Vortkamp.** 2002. Interaction of FGF, Ihh/Pthlh, and BMP signaling integrates chondrocyte proliferation and hypertrophic differentiation. Dev. Cell **3:**439–449.
27. **Miyaki, S., et al.** 2010. MicroRNA-140 plays dual roles in both cartilage development and homeostasis. Genes Dev. **24:**1173–1185.
28. **Murtaugh, L. C., L. Zeng, J. H. Chyung, and A. B. Lassar.** 2001. The chick

transcriptional repressor Nkx3.2 acts downstream of Shh to promote BMP-dependent axial chondrogenesis. Dev. Cell **1:**411–422.
29. **Nakamura, Y., et al.** 2007. The CCN family member Wisp3, mutant in progressive pseudorheumatoid dysplasia, modulates BMP and Wnt signaling. J. Clin. Invest. **117:**3075–3086.
30. **Nicolas, F. E., et al.** 2008. Experimental identification of microRNA-140 targets by silencing and overexpressing miR-140. RNA **14:**2513–2520.
31. **Ørom, U. A., and A. H. Lund.** 2010. Experimental identification of microRNA targets. Gene **451:**1–5.
32. **Ovchinnikov, D. A., J. M. Deng, G. Ogunrinu, and R. R. Behringer.** 2000. Col2a1-directed expression of Cre recombinase in differentiating chondrocytes in transgenic mice. Genesis **26:**145–146.
33. **Park, C. Y., Y. S. Choi, and M. T. McManus.** 2010. Analysis of microRNA knockouts in mice. Hum. Mol. Genet. **19:**R169–R175.
34. **Retting, K. N., B. Song, B. S. Yoon, and K. M. Lyons.** 2009. BMP canonical Smad signaling through Smad1 and Smad5 is required for endochondral bone formation. Development **136:**1093–1104.
35. **Rodríguez, C. I., et al.** 2000. High-efficiency deleter mice show that FLPe is an alternative to Cre-loxP. Nat. Genet. **25:**139–140.
36. **Schier, A. F., and W. S. Talbot.** 2005. Molecular genetics of axis formation in zebrafish. Annu. Rev. Genet. **39:**561–613.
37. **Tallquist, M. D., and P. Soriano.** 2003. Cell autonomous requirement for PDGFRalpha in populations of cranial and cardiac neural crest cells. Development **130:**507–518.
38. **Tuddenham, L., et al.** 2006. The cartilage specific microRNA-140 targets histone deacetylase 4 in mouse cells. FEBS Lett. **580:**4214–4217.
39. **Valencia-Sanchez, M. A., J. Liu, G. J. Hannon, and R. Parker.** 2006. Control of translation and mRNA degradation by miRNAs and siRNAs. Genes Dev. **20:**515–524.
40. **Wienholds, E., et al.** 2005. MicroRNA expression in zebrafish embryonic development. Science **309:**310–311.
41. **Yoon, B. S., et al.** 2005. Bmpr1a and Bmpr1b have overlapping functions and are essential for chondrogenesis *in vivo*. Proc. Natl. Acad. Sci. U. S. A. **102:**5062–5067.
42. **Zhang, L., et al.** 2007. Systematic identification of C. elegans miRISC proteins, miRNAs, and mRNA targets by their interactions with GW182 proteins AIN-1 and AIN-2. Mol. Cell **28:**598–613.